Monthly Notices
of the
ROYAL ASTRONOMICAL SOCIETY

Mon. Not. R. Astron. Soc. **413,** 1623–1632 (2011) doi:10.1111/j.1365-2966.2011.18235.x

Super-Eddington slim accretion discs with winds

Calanit Dotan★ and Nir J. Shaviv

Racah Institute of Physics, Hebrew University of Jerusalem, Jerusalem 91904, Israel

Accepted 2010 December 18. Received 2010 December 9; in original form 2010 April 11

ABSTRACT

We construct Super-Eddington Slim discs models around both stellar and supermassive black holes by allowing the formation of a porous layer with a reduced effective opacity. Unlike the standard scenario in which the discs become thick, super-Eddington discs remain slim. In addition, they accelerate a significant wind with a 'thick disc' geometry. We show that above about 1.5 times the standard critical mass accretion rate (needed to release the Eddington luminosity), the net luminosity released is above Eddington. At above about five times the standard critical rate, the central BH accretes more than the Eddington accretion rate. Above about $20\dot{m}_{\rm crit}$, the disc remains slim but the wind becomes spherical, and the present model breaks down.

Key words: accretion, accretion discs.

1 INTRODUCTION

The accretion of matter on to compact objects can often be described using the run-of-the-mill thin accretion disc model of Shakura & Sunyaev (1973, S&S). Because the accretion disc is optically thick, matter can radiate the potential energy it dissipates and remain cold, thus forming a geometrically 'thin' disc. The turbulent viscosity responsible for the dissipation is often described through the standard α-model, and it is also responsible for the transport of angular momentum outwards.

The S&S thin disc model applies to a wide range of conditions found in nature, however, when one of the underlying assumptions break down, so does the model.

At sufficiently low accretion rates, the disc becomes optically thin and it cannot radiate the energy dissipated. This energy is therefore advected with the flow, forming the so called Advection Dominated Accretion Flow (Ichimaru 1977; Narayan & Yi 1994; Abramowicz et al. 1995). Because the gas cannot cool, some of it can remain unbound (with a positive Bernoulli parameter) and easily produce significant outflows (Narayan & Yi 1994; Blandford & Begelman 1999; Shaviv, Wickramasinghe & Wehrse 1999).

The inability to radiate enough energy also arises for very high accretion rates. For sufficiently high rates, not only will the disc become radiation pressure dominated, it may become comparable to the Keplerian velocity squared. Such discs puff up to become 'slim' or 'thick' discs and advect the accretion energy with the flow (Paczynsky & Wiita 1980; Jaroszynski, Abramowicz & Paczynski 1980; Abramowicz et al. 1988).

More specifically, the energy release rate in a Keplerian disc, down to a radius r, is given by $GM_{\rm BH}\dot{m}/2r$, where $M_{\rm BH}$ is the black hole mass and $\dot{m}$ is the mass accretion rate. This energy should be compared to the Eddington luminosity of the BH, defined as

$$L_{\rm Edd} \equiv \frac{4\pi cGM_{\rm BH}}{\kappa}, \tag{1}$$

from which a critical accretion rate can be define to be

$$\dot{m}_{\rm crit} \equiv \frac{L_{\rm Edd}}{\eta_0 c^2}. \tag{2}$$

Here $\eta_0 = 1-\sqrt{8/9} \approx 0.057$ is the standard efficiency for accretion on to a Schwarzschild BH, obtained by calculating the energy of the last stable (circular) orbit (Bardeen 1973).

If $\dot{m}$ is large enough, that is, $\dot{m} \gtrsim \dot{m}_{\rm crit}$ then the energy released will approach the Eddington luminosity before reaching the inner radius of the disc. But, if the flux emitted by the disc is limited by the local Eddington flux, defined as

$$F_{\rm Edd} \equiv \frac{cGM_{\rm BH}z}{\kappa R^3}, \tag{3}$$

with $R \equiv \sqrt{r^2+z^2}$ (where r and z are the cylindrical coordinates), then the disc will not be able to radiate all the accretion energy. From that point inwards, the disc will become geometrically thick [having a scale height $H(r) \sim r$], and the excess energy will be advected inwards.

It is important to note that although the local flux in the disc does not surpass the Eddington flux, the overall luminosity can surpass the Eddington luminosity, simply due to the disc geometry (Jaroszynski et al. 1980; Paczynsky & Wiita 1980). Roughly, the Eddington luminosity can be surpassed by a factor of $\sim \ln r_{\rm out}/r_{\rm in}$, where $r_{\rm in}$ and $r_{\rm out}$ are the inner most stable orbit, the radius where the accretion energy is comparable to $L_{\rm Edd}$.

The aforementioned supercritical accretion discs to not include mass-loss, but mass-loss can take place. First, the discs can accelerate very luminous jets (Abramowicz & Piran 1980). Mass can also be blown away from the disc (Poutanen et al. 2007), as is seen to

★E-mail: calanit@phys.huji.ac.il

take place in numerical simulations (Eggum, Coroniti & Katz 1988; Ohsuga et al. 2005).

The above models assume, however, that the Eddington flux cannot be surpassed locally. It was shown that super-Eddinigton states do naturally arise in nature (Shaviv 2001b), allowing for high luminosities, while generating optically thick winds. It was shown numerically that such an opacity reduction does take place (Turner et al. 2005), and it was incorporated into a one-zone accretion model (Begelman 2006), showing how discs with significantly super-Eddington (SED) luminosities can exist.

Our goal in the present work is to consider the recent advances in the understanding of how SED atmospheres arise, what they look like, and the winds that they generate, and to incorporate these ideas into a model for very high accretion rate accretion discs. In Section 2, we begin by reviewing our present understanding of how SED states arise. In Section 3 we describe our model for SED accretion, and in Section 4 we describe the numerical solution. In Section 5 we describe the numerical results, and end with a discussion in Section 6.

2 BACKGROUND: SUPER-EDDINGTON STATES

We begin by reviewing the relevant physics pertaining to the emergence of SED states. These include three particular elements. First, the rise of inhomogeneities due to radiative hydrodynamic instabilities was shown to reduce the effective opacity (Shaviv 1998). This allows for the existence of SED atmospheres. Secondly, once a SED state arises, strong continuum driven winds are accelerated (Shaviv 2000, 2001b; Owocki, Gayley & Shaviv 2004). These optically thick winds are responsible for a significant mass-loss and are also important when determining the appearance of these objects. Last, if the wind mass-loss is too large, wind stagnation and a photon-tired state arises (Owocki & Gayley 1997; van Marle, Owocki & Shaviv 2009). In it, a layer is formed in which strong shocks mediate a high energy flux without an excessive mass flux. These three components are the necessary building blocks for the SED accretion disc models, and we therefore review them below.

2.1 The rise of super-Eddington states

According to common wisdom, objects cannot shine beyond their classical Eddington limit, $\mathcal{L}_{\rm Edd}$ (or locally beyond the Eddington flux, $\mathcal{F}_{\rm Edd}$, as is the case in accretion discs), since no hydrostatic solution exists. In other words, if objects do pass $\mathcal{F}_{\rm Edd}$, they are highly dynamic. They have no steady state, and a huge mass-loss should occur since their atmospheres are then gravitationally unbound and they should therefore be expelled. Thus, astrophysical objects according to this picture, can pass $\mathcal{L}_{\rm Edd}$ but only for a short duration corresponding to the time it takes them to dynamically stabilize once SED conditions arise.

For example, this can be seen in detailed 1D numerical simulations of thermonuclear runaways in classical nova eruptions, which can achieve SED luminosities but only for several dynamical time-scales (e.g. Starrfield 1989). However, once they do stabilize, they are expected and indeed do reach in the simulations, a sub-Eddington state. Namely, we naively expect to find no steady state SED atmospheres. This, however, is not the case in nature, where nova eruptions are clearly SED for durations which are orders of magnitude longer then their dynamical time-scale (Shaviv 2001b). This is exemplified with another clear SED object – the great eruption of the massive star η-Carinae, which was a few times above Eddington for over 20 yr (Shaviv 2000).

The existence of a SED state can be naturally explained, once we consider the following.

(i) Atmospheres become unstable as they approach the Eddington limit. In addition to instabilities that operate under various special conditions [e.g. Photon bubbles in strong magnetic fields (Arons 1992; Gammie 1998; Begelman 2002) or s-mode instability under special opacity laws (Glatzel 1994; Papaloizou et al. 1997)], two instabilities operate in Thomson scattering atmospheres (Shaviv 2001a). It implies that *all atmospheres* will become *unstable* already before reaching the *Eddington limit*.

(ii) The effective opacity for calculating the radiative force on an inhomogeneous atmosphere is not necessarily the microscopic opacity. Instead, it is given by

$$\kappa_V^{\rm eff} \equiv \frac{\langle F\kappa_V\rangle_V}{\langle F\rangle_V}, \tag{4}$$

where $\langle\,\rangle_V$ denotes volume averaging and F is the flux (Shaviv 1998). The situation is very similar to the Rosseland versus Force opacity means used in non-gray atmospheres, where the inhomogeneities are in frequency space as opposed to real space. For the special case of Thomson scattering, the effective opacity is always reduced.

Within the context of accretion discs, several particularly interesting results should be mentioned. Because strong magnetic fields are probably present, as they would naturally explain the viscosity through the MRI instability, the growth of magnetic photon bubbles were studied in the context of opacity reduction in accretion discs. Begelman (2002) has shown how shock trains in a system with a strong magnetic field will grow and decrease the effective opacity. The maximal opacity reduction possible was found to be of order the ratio between the magnetic pressure and the gas pressure. This, and other instabilities were later studied numerically in a radiative-MHD simulation of a column in a radiation-pressure dominated accretion disc (Turner et al. 2005). This analysis corroborated the analytical shock train results of Begelman (2002) and numerically found one instability predicted by Shaviv (2001a). Moreover, it is the first numerical demonstration how an atmosphere becomes porous and reduces its effective opacity. The analytical study of the magnetic photon bubbles in the context of discs was extended by Begelman (2006) where a one zone model was developed showing how accretion with a significantly SED luminosity can take place.

To conclude, we find that as atmospheres approach their classical Eddington limit, they will necessarily become inhomogeneous because of several possible instabilities. These inhomogeneities will unavoidably reduce their effective opacity such that the effective Eddington limit will not be surpassed even though the luminosity can be superclassical Eddington. This takes place in the external regions of luminous objects, where the radiation diffusion time-scale is shorter than the dynamical time-scale in the atmosphere. Further inside the atmosphere, convection is necessarily excited such that the total energy flux may be SED, but the radiative part of it is necessarily sub-Eddington with the convective flux carrying the excess (Joss, Salpeter & Ostriker 1973).

2.2 Super-Eddington winds

The atmospheres of SED objects, and SED accretion discs in particular, effectively remain sub-Eddington while being classically SED, only as long as the inhomogeneities comprising them are optically

thick. This condition will break at some point where the density is low enough. At this height, the effective opacity returns to its microscopic value and hence the radiative force becomes SED again. From this point outwards we obtain continuum driven winds. Because the winds are generally optically thick, the conditions in them affect the structure of the disc beneath.

At the critical point, the radiative and gravitational forces balance each other. This point will coincide with a sonic surface for a steady state wind (where the mass-loss velocity equals the local speed of sound). This allows us to obtain the local mass-loss rate per unit area, given by

$$\dot{\phi}_{\rm wind} = \rho_{\rm crit} v_{\rm s}(z_{\rm atm}) = \text{const.}, \tag{5}$$

where $z_{\rm atm}$ is the vertical height of the critical point, $\rho_{\rm crit}$ is the density at this point and $v_{\rm s}$ is the local speed of sound.

Based on the fact that instabilities develop structure with a typical size comparable to the density scale height in the atmosphere, it is possible to estimate the average density at the sonic point (Shaviv 2001b). Using this density, the mass-loss can be estimated to be

$$\dot{\phi}_{\rm wind} = \mathcal{W}\frac{F - \mathcal{F}_{\rm Edd}}{c v_{\rm s}}. \tag{6}$$

where $\mathcal{W}$ is a dimensionless wind 'function'. In principle, $\mathcal{W}$ can be calculated *ab initio* only after the non-linear state of the inhomogeneities is understood. This, however, is still lacking as it requires elaborate 3D numerical simulations of the non-linear steady state.

Nevertheless, deriving $\mathcal{W}$ can be achieved in several phenomenological models which depend on geometrical parameters such as the average size of the inhomogeneities in units of the scale height ($\zeta \equiv d/l_{\rm p}$), the average ratio between the surface area and volume of the blobs in units of the blob size (Ξ), and the volume filling factor f of the dense blobs. For example, in the limit in which the blobs are optically thick, one can show that $\mathcal{W} \approx 3\Xi/32\sqrt{\nu} f \zeta (1-f)^2$ (Shaviv 2001b), with ν being the ratio between the effective speed of sound in the atmosphere to the adiabatic one. Thus, $\mathcal{W}$ depends only on geometrical factors. It does not depend explicitly on the Eddington parameter $\Gamma \equiv L/\mathcal{L}_{\rm Edd}$ as long as the blobs have a single length scale. Once this assumption is alleviated, $\mathcal{W}$ can become a weak function of Γ (Owocki et al. 2004). Comparison to observations yields typical values of $\mathcal{W} \sim 1$–10 (Shaviv 2001b).

2.3 Photon-tired winds

An interesting modification to the above continuum driven winds arises when the predicted mass-loss is too high for the available luminosity to push it to $r \to \infty$. This happens when $v_{\rm esc} \gtrsim \sqrt{v_{\rm s} c/\mathcal{W}}$, and it gives rise to 'photon-tired winds' (Owocki & Gayley 1997). A wind solution with a monotonically decreasing velocity is then not possible, because the wind stagnates at a finite radius.

The behaviour of photon tired winds was studied by van Marle et al. (2009). It was found that shocks form between infalling material and the outflowing wind. This forms a layer of shocks in which there is a large kinetic flux, but without the associated mass flux. When photon tired winds arise, the mass-loss from the top of the layer of shocks is reduced to less than the photon tired limit, and the luminosity to less than the Eddington luminosity.

3 THE MODEL

Our goal is to construct SED accretion discs, namely, discs which radiate fluxes that can locally exceed the Eddington flux. We look for slim disc solutions which are heuristically described in Fig. 1. More specifically, we have to consider the following points.

(i) *Geometry*: Although in principle, one could envision SED accretion solutions with different geometries, we look for disc like solutions. We shall assume that the vertical length scale is sufficiently smaller than the radius, such that we can deconstruct the problem into vertical and radial components. As we shall see below, the hydrostatic part of the disc satisfies this conditions except for the highest accretion rates. Note that because the vertical structure is not *much* smaller, the geometry is not that of a thin disc, but that of a slim disc. This also implies that we cannot assume Keplerian velocities.

(ii) *Porosity*: As mentioned above, high radiative fluxes give rise to porosity which reduces the effective opacity, thereby allowing

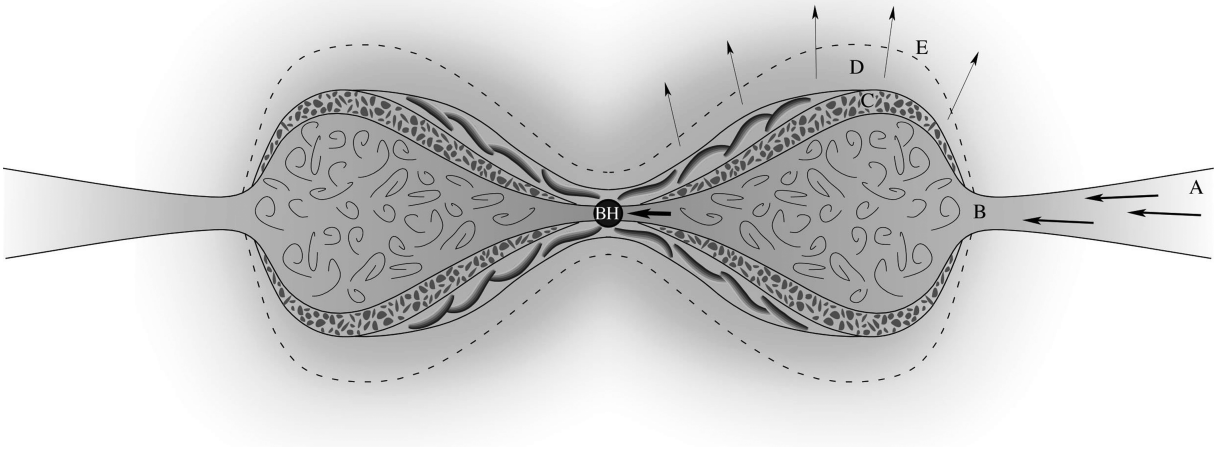

Figure 1. The model structure. The different regions are: (A) A sub-Eddington thin disc (following the solution of S&S). (B) At some point, the disc becomes radiation-pressure dominated. Further inside, somewhat outwards of the region where the energy release corresponds to the Eddington luminosity, the disc begins to inflate and lose its thin geometry. Once SED states are allowed to arise, the standard thick disc picture is modified. (C) A porous layer forms at the less dense regions above the convection layer. (D) At a height were the porous structure become optically thin, a wind is accelerated. (E) Since it is optically thick, the photosphere is located in the wind itself. (F) In the inner parts of the disc, the escape velocity is large enough to give rise to a photon tired layer, which effectively moves the sonic point higher.

the existence of SED fluxes in the hydrostatic atmospheres. Thus, a necessary component of our model is an opacity law of the form $\kappa(\Gamma)$, which takes the porosity into account.

(iii) *Convection*: Joss et al. (1973) have shown that high radiative fluxes give rise to convection as the radiative fluxes approach the Eddington limit. The dense inner parts of the SED disc, near the equatorial plane are therefore expected to be convective.

(iv) *Wind*: Since a porous atmosphere can reduce the opacity only as long as the inhomogeneities comprising it are optically thick, a necessary outcome of SED atmospheres is the acceleration of continuum driven winds where the average density is low enough. Because this mass-loss can be significant, it has two interesting ramifications. First, because the wind is generally optically thick, the photosphere is going to reside in the wind. This will have various observational consequences. Secondly, the mass accretion rate decreases as the radius decreases.

3.1 Radial structure

As mentioned above, the small thickness of the disc enables the separation between the radial structure and the vertical one. The equations describing the radial structure are obtained from the radial conservation of mass, radial momentum, energy, and angular momentum. An additional equation is the closure relation for the stress tensor.

Radial mass conservation gives

$$\frac{\mathrm{d}\dot{m}}{\mathrm{d}r} = 4\pi r \dot{\phi}_{\mathrm{wind}}, \tag{7}$$

where

$$\dot{m} = 4\pi r v_r \int_0^H \rho \, \mathrm{d}z \tag{8}$$

is the mass accretion rate. Note that we assume a height independent velocity structure.

Conservation of radial momentum gives

$$v_r \frac{\mathrm{d}v_r}{\mathrm{d}r} + \frac{1}{\rho}\frac{\mathrm{d}P}{\mathrm{d}r} = -\frac{\partial \Psi}{\partial r}, \tag{9}$$

where Ψ is a pseudo-Newtonian potential given by Paczynsky & Wiita (1980) as

$$\Psi = -\frac{GM_{\mathrm{BH}}}{R - rg}, \tag{10}$$

and $R = \sqrt{r^2 + z^2}$. For the radial structure, we assume that $z = 0$.

The equation for angular momentum conservation is

$$\rho v_r \frac{\mathrm{d}}{\mathrm{d}r}(r^2\omega) = -\frac{1}{r}\frac{\mathrm{d}}{\mathrm{d}r}\left(r^2 \tau_{r\phi}\right), \tag{11}$$

where $\tau_{r\phi}$ is the tangential stress. Following the standard 'α' prescription, we write:

$$\tau_{r\phi} = -\alpha P. \tag{12}$$

The heat produced by the viscosity is partly radiated away (locally), and partly transferred by advection into smaller radii. The radial heat advection is given by the difference between the amount of heat being produced by the viscosity, and the energy radiated away from the surface of the disc, that is,

$$T\frac{\mathrm{d}s}{\mathrm{d}r} = (F - \Phi)\frac{4\pi r}{\dot{m}}, \tag{13}$$

where s is the specific entropy, F is the flux radiated from the surface, while Φ is the dissipation function, given by

$$\Phi = r\frac{\mathrm{d}\omega}{\mathrm{d}r}\int_0^{z_0} \tau_{r\phi}\, \mathrm{d}z. \tag{14}$$

Note that the specific entropy increases with decreasing radii in the case of advection, hence $\mathrm{d}s/\mathrm{d}r < 0$. However, another possibility exists, in which the infalling matter releases part of its heat (i.e. $\mathrm{d}s/\mathrm{d}r > 0$). This heat, together with the heat generated by the viscosity, is radiated away. This process dominates the inner radii region of the accretion flow, as we will show in the results.

3.1.1 Inner sonic point

At large radii, the radial velocity is very small when compared to the speed of sound, while matter is freely infalling at the vicinity of the BH. This implies that at some radius $r = r_{\mathrm{s}}$, the radial velocity should become equal to the speed of sound, and then exceed it. Similarly to the case of spherical Bondi accretion, we can obtain the condition for this point. Because of the radial pressure gradient, this point will reside between the last stable orbit $r_{\mathrm{ls}} = 3r_{\mathrm{g}}$ and the marginally stable orbit, $r_{\mathrm{ms}} = 2r_{\mathrm{g}}$. Using equations (8) and (9), and that

$$\frac{\mathrm{d}p}{\mathrm{d}r} = \frac{\partial p}{\partial s}\frac{\mathrm{d}s}{\mathrm{d}r} + \frac{\partial p}{\partial \rho}\frac{\mathrm{d}\rho}{\mathrm{d}r} = \frac{p}{s}\left(\frac{4}{3} - \beta\right)\frac{\mathrm{d}s}{\mathrm{d}r} + v_{\mathrm{s}}^2\frac{\mathrm{d}\rho}{\mathrm{d}r}, \tag{15}$$

where $v_{\mathrm{s}}^2 \equiv \partial p/\partial\rho$ and s is the specific entropy, we obtain

$$\frac{v_r^2 - v_{\mathrm{s}}^2}{v_r}\frac{\mathrm{d}v_r}{\mathrm{d}r} \simeq \frac{1}{r}\left[v_{\mathrm{s}}^2 + (v_\phi^2 - v_{\mathrm{kep}}^2)\right] - \frac{\partial p}{\partial s}\frac{\mathrm{d}s}{\mathrm{d}r}\frac{1}{\rho}. \tag{16}$$

Note that we have assumed the following approximation, that

$$\frac{1}{\Sigma}\frac{\mathrm{d}\Sigma}{\mathrm{d}r} \approx \frac{1}{\rho}\frac{\mathrm{d}\rho}{\mathrm{d}r}, \tag{17}$$

where $\Sigma \equiv \int \rho \mathrm{d}z$. At the sonic radius $v_r = v_{\mathrm{s}}$, such that the r.h.s. of equation (16) must vanish, i.e. at the sonic radius we have that

$$v_{\mathrm{s}}^2 + \left(v_\phi^2 - v_{\mathrm{kep}}^2\right) \simeq r\frac{\partial p}{\partial s}\frac{\mathrm{d}s}{\mathrm{d}r}\frac{1}{\rho}. \tag{18}$$

We use this expression as the inner boundary condition for the disc.

3.2 Vertical structure

The vertical structure of the SED accretion disc can be divided into two regions, a hydrostatic region which includes also the porous atmosphere, and the region of a continuum driven wind. Because the wind is optically thick, the thermal conditions at the wind affect the hydrostatic structure. This is unlike typical stellar systems with optically thin winds. As a consequence, the hydrostatic structure has to be solved together with the wind, though the governing equations are different for the two regions.

3.2.1 Hydrostatic region

In the hydrostatic region, any energy which is generated by the viscosity and not advected radially, is transported in the vertical direction through either convection or radiative transfer, or both.

The first equation describing this region is that of hydrostatic equilibrium,

$$\frac{1}{\rho}\frac{\mathrm{d}P}{\mathrm{d}z} = -\frac{\mathrm{d}\Psi}{\mathrm{d}z}. \tag{19}$$

The temperature gradient is determined according to the energy transfer mechanism. It is given by

$$\frac{\mathrm{d}T}{\mathrm{d}z} = \begin{cases} \dfrac{\gamma - 1}{\gamma}\dfrac{\mathrm{d}P}{\mathrm{d}z}\dfrac{T}{P}, & \text{in the convective zone,} \\ -\dfrac{3\kappa_{\mathrm{eff}}\rho F}{4acT^3}, & \text{in the radiative zone,} \end{cases} \tag{20}$$

where ρ is the density, F is the vertical radiative flux and γ is the adiabatic index. Convection is present if the standard Schwarzschild criterion is satisfied. But for convection to be efficient, the convective flux must be smaller than the maximum possible which is given by

$$F_{\rm conv,max} = \rho v_{\rm s}^3, \tag{21}$$

and $v_{\rm s}$ is the adiabatic speed of sound.

We assume that the underlying microscopic opacity is that of Thomson scattering. However, as discussed in Section 2, we expect that the very high radiative flux in the region where convection is ineffective will give rise to radiative hydrodynamic or radiative magneto-hydrodynamic instabilities. Once non-linear, the instabilities will be responsible for a reduction in the effective opacity. However, since there are yet no systematic numerical simulations quantifying the opacity reduction as a function of the flux, nor are there yet empirical constraints (e.g. through the modelling of classical nova eruptions), we have no option but to assume an ad hoc relation between the effective Eddington factor $\Gamma_{\rm eff} \equiv F/\mathcal{F}_{\rm eff}$ and the classical Eddington factor $\Gamma \equiv F/\mathcal{F}_{\rm Edd}$. As we shall see in Section 5.3, the various observable disc characteristics are rather insensitive to the exact effective opacity law considered. This is similar to the fact that the observable disc properties are insensitive to the choice of α.

Notwithstanding, we do have some constraints on the opacity law. We require a relation for which the effective opacity returns to its microscopic value at small fluxes. The behaviour at high fluxes is less certain. If for example there is a maximum possible density contrast between the low and high density regions, then there will be a maximum luminosity above which $\Gamma_{\rm eff} > 1$. If magnetic photon bubbles are responsible for the inhomogeneities, then the highest flux will be roughly given by the ratio between the magnetic and gas pressures (Begelman 2002; Turner et al. 2005). Nevertheless, we know empirically that the envelope of Nova LMC 1991 was dynamically stable while radiating with $L \gtrsim 10 L_{\rm Edd}$ (Schwarz et al. 2001). If we add the mechanical flux, the luminosity at the base of the wind probably reached as much as $20 L_{\rm Edd}$. Thus, if there is a Γ above which $\Gamma_{\rm eff} > 1$, it takes place for at least $\Gamma \gtrsim 20$. In our models we barely reach such high fluxes. We can therefore assume an opacity law for which $\Gamma_{\rm eff}$ reaches unity only asymptotically.

Another point to consider is whether the deviation of the effective opacity from the microscopic value takes place only above a critical $\Gamma_{\rm crit}$, which may cause a discontinuity in the derivative of the opacity law, or whether the deviation is more gradual. If magnetic photon-bubbles are responsible for the inhomogeneities, then their effect will gradually increase as the radiation pressure becomes more important (e.g. Begelman 2002). If on the other hand the magnetic field is weak, other instabilities may set in only above a critical $\Gamma_{\rm crit}$ (Shaviv 2001a). Since magnetic fields are expected to be important in accretion discs, we therefore choose a 'gradual' opacity law.

Given the above, we assume that the relation between the effective Eddington factor $\Gamma_{\rm eff} \equiv F/\mathcal{F}_{\rm eff}$ and the classical Eddington factor $\Gamma \equiv F/\mathcal{F}_{\rm Edd}$ is empirically given by

$$\Gamma_{\rm eff} = \frac{1}{(1+\Gamma^p)^{1/p}}. \tag{22}$$

Here p is a free parameter, which we keep to be $p = 2$, except for the sensitivity analysis in Section 5.3.

3.2.2 *Continuum driven winds*

As described in Section 2.2, a continuum driven wind is accelerated from the region where the density is low enough, such that the inhomogeneity based opacity reduction becomes inefficient. In this region, the effective opacity approaches the microscopic value, such that the radiative flux is again SED.

The primary equations describing the wind structure are the equation of motion

$$\rho v_z \frac{{\rm d}v_z}{{\rm d}z} = -\frac{{\rm d}P}{{\rm d}z} - \rho g_z, \tag{23}$$

where $g_z = -\partial\Psi/\partial z$, and the energy conservation equation

$$F(z) = F_{\rm atm} - \dot{\phi}_{\rm wind}\left(\frac{v_z^2}{2} + \frac{GM_{\rm BH}}{R_{\rm atm}} - \frac{GM_{\rm BH}}{R}\right). \tag{24}$$

The index 'atm' denote values at the top of the hydrostatic atmosphere beneath the wind. Note that we assume here that the wind geometry is that of a slab. Namely, we assume that $z \ll R$. This assumption breaks down for high accretion rates, at which point the present solution fails.

From the last two equations, and the assumption that $\kappa = {\rm const.}$, we derive the radiative flux and wind velocity as a function of z:

$$F(z) = F_{\rm atm}\exp\left(\frac{\kappa\dot{\phi}_{\rm wind}(z_{\rm atm}-z)}{c}\right), \tag{25}$$

$$\frac{v_z^2}{2} = \frac{GM_{\rm BH}}{R_{\rm atm}}\left[\frac{1}{m}\left(1-\frac{F(z)}{F_{\rm atm}}\right) + \left(\frac{R_{\rm atm}}{R}-1\right)\right] + \frac{v_{\rm s}^2}{2}, \tag{26}$$

where

$$m \equiv \frac{\dot{\phi}_{\rm wind} GM_{\rm BH}/R_{\rm atm}}{F_{\rm atm}}. \tag{27}$$

m is the ratio between the energy flux needed to accelerate the wind out of the gravitational potential well, and the radiation flux provided to the wind by the system.

Another aspect of this thick wind is the location of the photosphere. While in the slim and thin disc models the photosphere resides where the gas becomes optically thin, in our case, the photosphere resides much higher, where the wind becomes optically thin. The optical depth of the wind is given by

$$\tau = \int_{z_{\rm atm}}^{\infty} \kappa\rho\,{\rm d}z. \tag{28}$$

Note also that the change in the location of the photosphere is accompanied by a decrease in the radiative flux emitted from the disc (as energy is used to accelerate the wind), hence, a decrease in the effective temperature.

As described in Section 5, the typical ratio we obtain between the height of the photosphere and the radius is small, that is, $z_{\rm ph}(r)/r \lesssim 1$, as long as the accretion rates are not too large, i.e. $\dot{m} \lesssim 20\dot{m}_{\rm crit}$. For higher accretion rates, the wind geometry ceases to be disc-like, and the solution described here breaks down.

3.2.3 *Photon tired winds*

As elaborated upon in Section 2.3, photon tired winds are formed when the available radiative flux at the sonic point is insufficient to drive the mass-loss driven at the sonic point out of the gravitational potential well (see Owocki & Gayley 1997). Under such conditions, a layer of shocks forms in which the effective sonic point moves

upwards, and reduces the actual mass-loss. Using the results from van Marle et al. (2009), we empirically model the actual $\dot{\phi}_{\rm wind}$ to be,

$$\frac{\dot{\phi}_{\rm wind}}{\dot{\phi}_{\rm tiring}} \simeq \max\left(0.2\left(\frac{F}{F_{\rm Edd}}\right)^{0.6}, 0.9\right), \quad (29)$$

where $\dot{\phi}_{\rm tiring} \equiv F/(GM_{\rm BH}/R_{\rm atm})$, if it is smaller than $\dot{\phi}_{\rm wind}$ obtained when photon tiring is unimportant (and given by equation 6).

3.2.4 Boundary conditions

The vertical structure of the disc is determined by the local equatorial conditions, i.e. the total pressure $P(r, z = 0)$ and the density $\rho(r, z = 0)$. The total radiative flux is a free variable. It is determined by the vertical structure which has to be solved for given the top boundary condition for the radiation field. The latter is the blackbody radiation law,

$$F(r, z_0) = \sigma T_{\rm eff}^4. \quad (30)$$

Here $T_{\rm eff}$ is the temperature at optical depth $\tau = 2/3$, as obtained by the outward integration.

4 NUMERICAL SOLUTION

The problem we are required to solve is divided into two parts, vertical and radial integration. Each radial integration step is accompanied by a vertical integration.

For the vertical integration we take an initial guess for the radiative flux and solve equations (19) and (20) for the hydrostatic part, and equations (23) and (24) for the wind (equations are integrated using the forth order Runge–Kutta method), and the validity of the boundary condition (equation 30) is checked. This vertical integration is repeated with different values for the radiative flux (using the shooting method) until equation (30) is fulfilled.

Using the emitted flux F, the mass-loss rate $4\pi r\dot{\phi}_{\rm wind}{\rm d}r$ and the vertical integrations over the pressure and the density, equations (7)–(9), (11) and (13) are solved. This integration is taken up to the inner sonic radius (where $v_r = v_{\rm s}$), which should reside between $r_{\rm ls}$ and $r_{\rm mb}$. The location of the sonic point is determined by the initial guess for the outer pressure, $p(r_{\rm out}, 0)$. A shooting method is used to determined the outer pressure.

5 RESULTS

In this section we present the results for accretion discs with $\alpha = 0.001$ around a stellar BH of mass $10\,{\rm M}_\odot$ and around a supermassive BH of mass $10^{6.5}\,{\rm M}_\odot$. We define the *outer accretion rate* as the rate of mass entering the disc at large radii before any mass-loss takes place.

For the stellar BHs, we take outer accretion rates of 1, 5, 10 and $20\dot{m}_{\rm crit}$. We find that the discs lose considerable amounts of mass through a wind, such that the real accretion rates (= mass passing the sonic radius per unit time, $\dot{m}_{\rm real}$) are 0.7, 2.4, 3.8 and 5.9, respectively, i.e, in stellar BHs with outer accretion rates $\dot{\rm m} \gtrsim 5\dot{m}_{\rm crit}$ more than half of the mass entering the accretion disc in the outer radius will not be accreted into the black hole but leave as a wind. Mass accretion rates as a function of the radius are shown in Fig. 2. The vertical heights of the discs are given in Fig. 3, where thin lines denote the location of the photosphere inside the wind, while the thick lines denote the sonic surface (the base of the wind). At large radii, where the wind is absent, thick lines give the heights of the photosphere as well. Note that it is impossible to obtain a situation in which all the mass accelerates in a wind since part of the energy is used to heat the gas, implying that without any net accretion, there will be an insufficient amount of energy to drive the matter back to infinity.

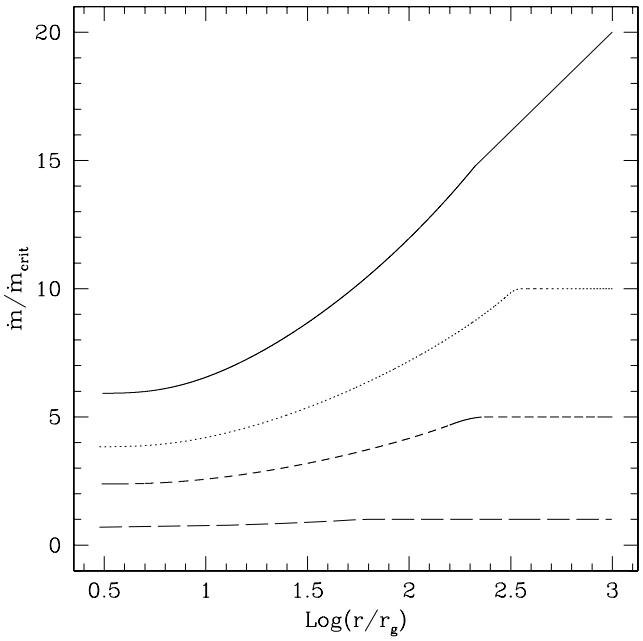

Figure 2. The mass accretion rate (in units of the critical rate, $\dot{m}/\dot{m}_{\rm crit}$) as a function of radius, for different outer accretion rates on to a BH with $M_{\rm bh} = 10\,{\rm M}_\odot$. From top to bottom, the lines denote accretion of $20\dot{m}_{\rm crit}$ (solid line), $10\dot{m}_{\rm crit}$ (dotted line), $5\dot{m}_{\rm crit}$ (short dashed) and accretion of $\dot{m}_{\rm crit}$ (long dashed line).

The gas to total pressure ratio, β in the equatorial plane ($z = 0$), is shown in Fig. 4. Apparently, the gas pressure dominates at large radii. However, radiation pressure becomes progressively more important at smaller radii. Radiation pressure is also dominant for higher accretion rates. Close to the radial sonic point the gas pressure becomes important again.

5.1 Efficiency of accretion

The efficiency of accretion is defined by

$$\eta = \frac{L}{\dot{m}c^2}. \quad (31)$$

Substituting $\dot{m}_{\rm real}$ into equation (31), we obtain the accretion efficiencies (see Table 1). For low accretion rates, the efficiency is slightly higher than the pseudo-Newtonian η_0 case because the wind is optically thin, while for higher accretion rates the wind is optically thick and $\eta/\eta_0 < 1$.

5.2 Spectra and luminosities

The total luminosities leaving the discs in units of Eddington luminosity are 0.8, 2.5, 4.1 and 5.1, respectively. Thus, for outer accretion rates of about $1.5\dot{m}_{\rm crit}$, the total radiated luminosity exceeds the Eddington 'limit'.

The accumulated luminosity $L(r) = \int_{r_{\rm out}}^{r} 4\pi r F(r){\rm d}r$ is shown in Fig. 5. Assuming a local Planck distribution and using the effective temperature $T_{\rm eff}(r)$, the emergent luminosity per unit frequency,

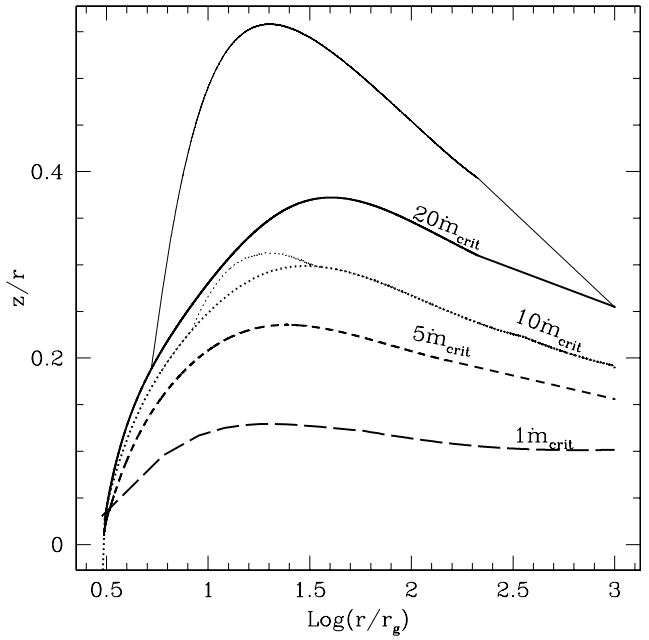

Figure 3. The vertical height (z/r) of the disc as a function of radius, for the same accretion rates as before. The thick lines denote the position of the photosphere when a wind is absent, while the thin lines denote the photosphere in the optically thick wind when present, in which case the thick line denotes the location of the sonic surface at the base of the wind. The line types are as before (top to bottom, they denote the $20\dot{m}_{\rm crit}$, $10\dot{m}_{\rm crit}$, $5\dot{m}_{\rm crit}$ and $\dot{m}_{\rm crit}$ cases). Note that for the two lower accretion rate $\dot{m} = \dot{m}_{\rm crit}$ and $\dot{m} = 5\dot{m}_{\rm crit}$ the wind is always optically thin and the photosphere coincides with the sonic point of the wind for all radii.

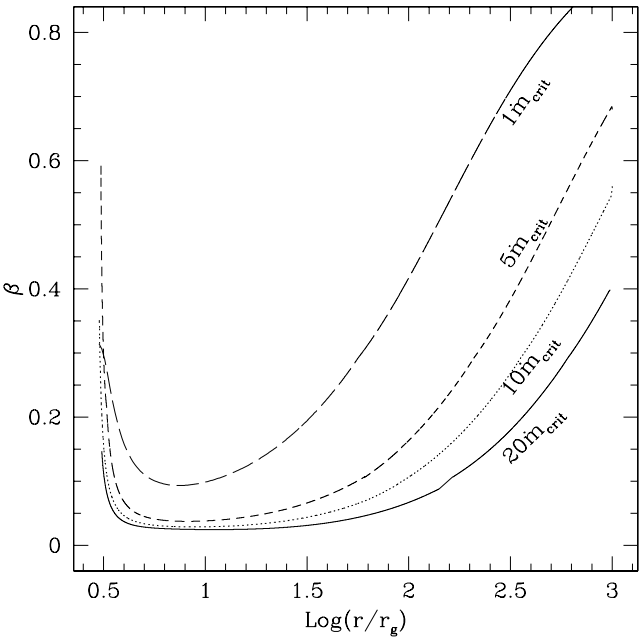

Figure 4. The ratio $\beta \equiv P_{\rm g}/P_{\rm tot}$ versus $\log(r/r_{\rm g})$ (bottom to top, the lines denote the $20\dot{m}_{\rm crit}$, $10\dot{m}_{\rm crit}$, $5\dot{m}_{\rm crit}$ and $\dot{m}_{\rm crit}$ cases). At large radii, the solutions approach the standard Shakura–Sunyaev solution, and the radiation pressure is less important. Closer to the black hole, the radiation pressure becomes more important and the radiative flux increases. Near the inner radial sonic point $\mathrm{d}s/\mathrm{d}r > 0$, and the gas pressure becomes important again.

L_ν, is

$$L_\nu = \pi \int_{r_{\rm s}}^{r_{\rm out}} 4\pi r\, B_\nu(T_{\rm eff}(r))\, \mathrm{d}r \qquad (32)$$

where B_ν is Planck function. This is given in Fig. 6. It should be emphasized that additional effects are likely to modify the outgoing radiation, implying that the blackbody approximation is probably a very bad approximation for the outgoing spectra. For example, there might not be sufficient absorption in the scattering dominated atmospheres to thermalize the emission at all frequencies (e.g. Davis et al. 2005). Likewise, a hot plasma above the disc will comptonize the spectrum (e.g. Titarchuk 1994). Reasonable modelling of the radiated spectra therefore requires an extended analysis that is beyond the scope of this work.

Table 1 summarizes the above results.

Table 1. Summary of the slim accretion discs around $10\,{\rm M}_\odot$ with $\alpha = 0.001$. The mass accretion rates are given in units of the critical rate while the luminosity and energy dissipation (which is the total energy produced by viscosity) are given in units of the Eddington luminosity of the BH. The last column is the efficiency of the disc compared to the standard disc efficiency (see equation 2), calculated with the *real* accretion rate. The efficiency calculated using the *outer* accretion rate is smaller. At high accretion rates, a significant wind is accelerated, taking some of the energy and reducing the efficiency.

$\dot{m}_{\rm out}/\dot{m}_{\rm crit}$	$\dot{m}_{\rm real}/\dot{m}_{\rm crit}$	$L_{\rm tot}/\mathcal{L}_{\rm Edd}$	Energy dissipation	Efficiency (η/η_0)
1	0.70	0.79	0.79	1.12
5	2.4	2.5	2.6	1.06
10	3.8	4.1	4.2	1.06
20	5.9	5.1	6.5	0.87

5.3 Sensitivity to model parameters

There are two primary uncertainties in our model. The first is in the basis of all α-disc models, the α parameter. The second uncertainty is the exact structure of the porous atmosphere which determines the value of the effective opacity. Figs 7–9 demonstrate how the $10\dot{m}_{\rm crit}$ on to a $10\,{\rm M}_\odot$ BH model varies when choosing different model parameters.

The figures depict the results of models using three different values of $\alpha, \alpha = 0.001$, 0.01 and 0.1. One can see that increasing the α-parameter by a factor of 10, decreases the total luminosity and the real mass accretion rate by approximately 10 per cent. The only large effect that the increase of α has is the slimming down of the disc, reducing it from $z/r \approx 0.3$ at its maximum for $\alpha = 0.001$ to $z/r \approx 0.17$ for $\alpha = 0.001$. However, the disc's width is not directly observable.

The effective opacity law we used is given by equation 22, where p is a free parameter. We also considered other opacity laws, all giving relatively similar results. Plotted in the figures are the results of the $p = 3$ case, which had the largest effect. Increasing p implies that the porous atmosphere is less effective at reducing the effective opacity. Here the disc puffs up by 40 per cent, however, the accretion rate increased by only 7 per cent and the total luminosity, by about 12 per cent.

In summary, the theoretical uncertainties in the model do not translate into large uncertainties in the model predictions. The only variable which is sensitive is the total disc width. Although this cannot be directly observed, it does have an interesting ramification.

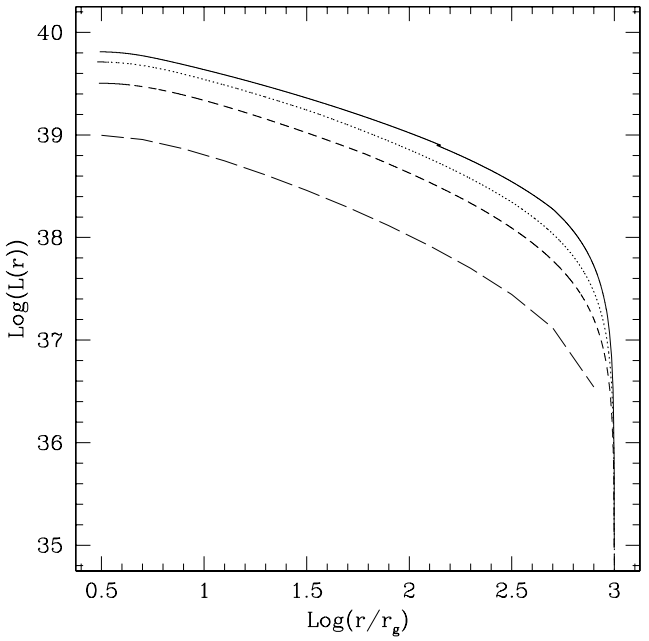

Figure 5. Radially integrated luminosity $L(r)$ in erg s^{-1} (integrated from an outer radius of $10^3 r_s$) versus $\log(r/r_g)$ for the four models (top to bottom, the lines denote the $20\dot{m}_{crit}$, $10\dot{m}_{crit}$, $5\dot{m}_{crit}$ and $\dot{m}_{crit}$ cases).

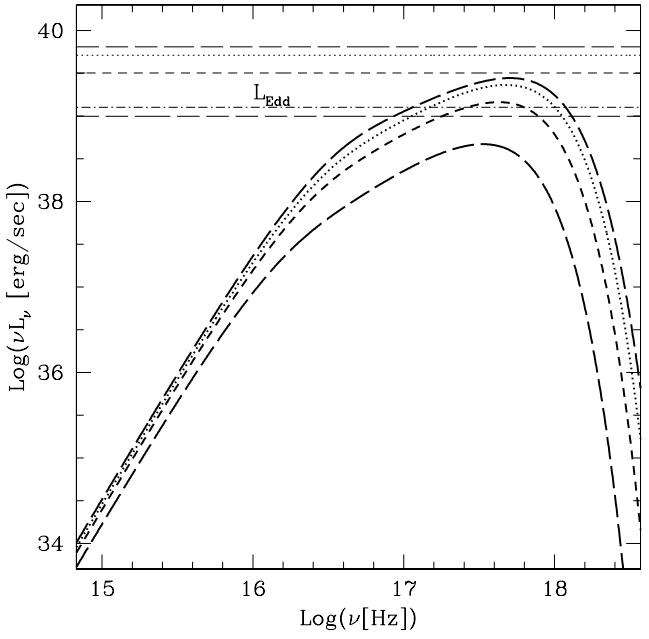

Figure 6. The total luminosity $\log(\nu L_\nu)$ versus $\log(\nu)$, for the same discs as before (top to bottom, the lines denote the $20\dot{m}_{crit}$, $10\dot{m}_{crit}$, $5\dot{m}_{crit}$ and $\dot{m}_{crit}$ cases, respectively). The horizontal lines depict the total radiated luminosity. The additional horizontal line (dot–dashed) is the Eddington luminosity. Note that the model assumes a Planckian spectrum at each radius, which is likely to be a terrible approximation.

Our model breaks down when the wind is not slim anymore, giving rise to winds with spherical geometry. This implies that the highest $\dot{m}$ and the highest L which can be achieved with this model is parameter dependent. Larger values of α and larger opacity reductions will give higher maximal rates.

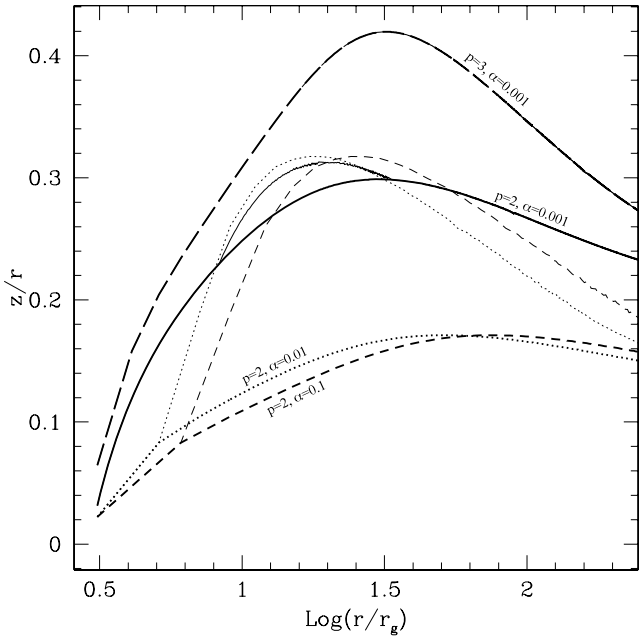

Figure 7. Comparison between the vertical structure, z/r, of discs with different atmospheric effective opacities and different α, for $10\dot{m}_{crit}$ around $M_{BH} = 10\,M_\odot$. The solid and long dashed lines describe models with opacity laws having $p = 2$ and 3, respectively, while $\alpha = 0.001$. The dotted and dashed lines describe models which have $\alpha = 0.01$ and 0.1, respectively, while $p = 2$. Thick lines depict the height of the photosphere when an optically thick wind is absent or the sonic point when such a wind is present. Thin lines mark the height of the photosphere when present in a thick wind.

5.4 Super massive BH

In addition to accretion discs around a stellar BH, we also examined super critical accretion around a super massive BH of mass $10^{6.5}\,M_\odot$, with outer accretion rates of 10 and $20\dot{m}_{crit}$.

We find that the real accretion rates for these discs are slightly smaller when compared to the stellar BH case, $2.6\dot{m}_{crit}$ and $3.8\dot{m}_{crit,}$ respectively. This gives rise to slightly reduced total luminosities, of 2.9 and $3.7L_{Edd}$ for the two cases (as compared with 3.9 and $4.9L_{Edd}$ for the equivalent accretion on to the stellar BH). The relative vertical height (z/r) is smaller as well (reaching a maximum value of $z/r \approx 0.55$ for the $\dot{m}_{out} = 20\dot{m}_{crit}$, as compared to $z/r \approx 0.65$ in the equivalent stellar BH case. Fig. 10 shows the spectra from these discs.

5.5 Comparison to other models

It is interesting to compare the results to other high accretion rate models. In particular, we can compare the results to those of Poutanen et al. (2007) who, like the present analysis, constructed steady state 1+1D models which include both advection and winds, and to Ohsuga et al. (2005), who carried out 2D-RHD simulations of high accretion rate discs.

The first point to note is demonstrated in Fig 11. The models which include porous atmospheres allow larger total radiative fluxes from lower accretion rates. In fact, the same luminosity can be obtained with an $\dot{m}$ which is typically 10 times smaller than the $\dot{m}$ in standard models. This is because the standard models are locally limited by the Eddington flux, which in a disc geometry can be integrated to $\sim \ln(\dot{m}/\dot{m}_{crit})$. However, once we allow the formation of a porous layer, we can locally surpass the Eddington flux, and

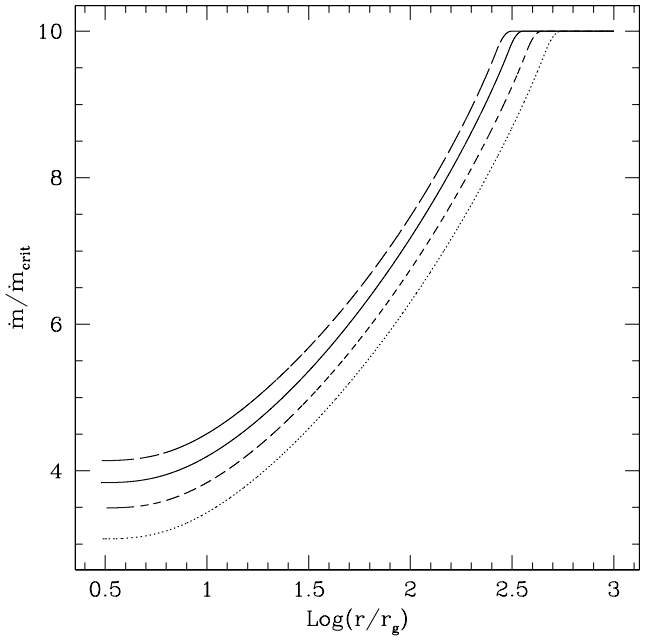

Figure 8. Comparison between the accretion rates of discs with different atmospheric effective opacity parameters and different values of α, as labeled in Fig. 7. Overall, the different models have very similar mass-losses, even though the opacities and viscosities vary considerably.

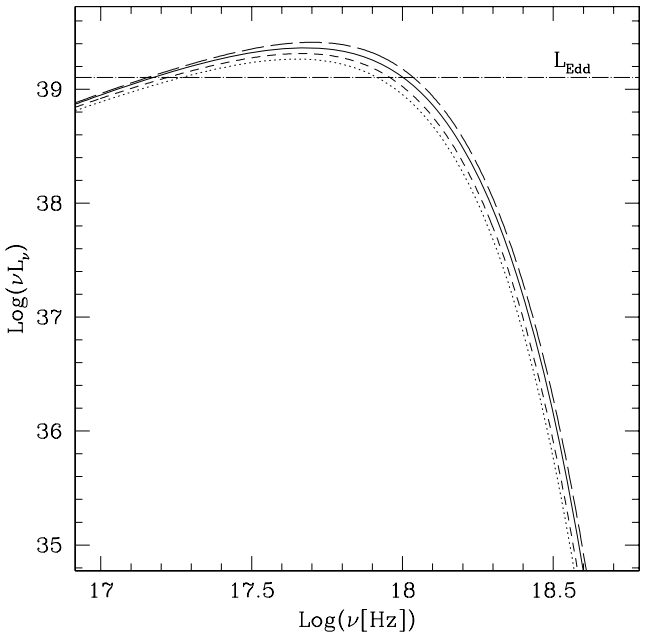

Figure 9. Comparison between the spectra, $\log(\nu L_\nu$ [erg s^{-1}]) versus $\log(\nu$[Hz]), for the different models given in Fig. 7.

obtain integrated fluxes which are higher, and without losing as much mass in the wind.

A more careful comparison reveals that the porous layer gives rise to a secondary effect allowing higher fluxes. Because radiation can escape more easily through the porous layer, less energy is advected with the flow. For this reason, we obtain radiating efficiencies from the actually accreted mass, which are close to that expected from the thin disc, about 6 per cent. However, in the models of Ohsuga et al. (2005), the typical efficiencies are lower, only 1 per cent to 3

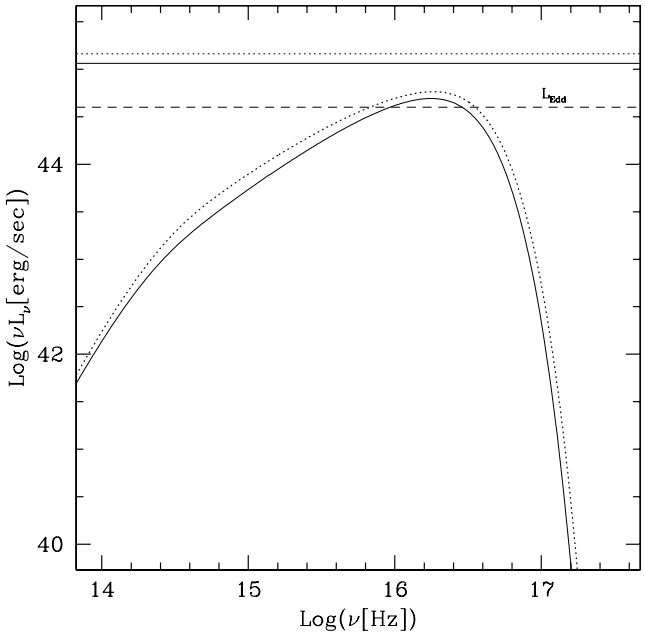

Figure 10. The emitted spectra, $\log(\nu L_\nu$ [erg s^{-1}]) versus $\log(\nu$[Hz]), by accretion discs on to a supermassive BH, with a mass of $10^{6.5}$ M$_\odot$. The outer accretion rates are $10\dot{m}_{\rm crit}$ (solid line) and $20\dot{m}_{\rm crit}$ (dotted line). The horizontal thin lines are the total luminosities and dashed line is the Eddington luminosity for comparison.

per cent. In other words, discs with porous atmospheres are brighter because more mass can actually reach the BH and more energy is extracted per gram, from this mass.

6 DISCUSSION

In the present analysis, we searched numerically for possible solutions describing super-critical accretion discs around black holes, while allowing for the formation of 'porous' layers with a reduced opacity. We found solutions with significantly super-critical accretion rates, in which the vertical disc height is smaller than the radius, that is, *slim* discs. Because the SED state excites a strong wind, the actual mass accretion on to the BH can be notably smaller. Solutions were found to exist with accretion rates ranging between about $0.5\dot{m}_{\rm crit}$ to about $20\dot{m}_{\rm crit}$. In all cases, there is a photon tired continuum driven wind.

At the low range, the discs are overall sub-Eddington, but locally the flux can surpass the critical value, and therefore it can excite continuum driven winds. Namely, the critical accretion rate given by equation (2) is not the lower limit for wind generation. At the low range, almost all the energy dissipated is either radiated away or transferred to the wind. Moreover, the wind is then optically thin and the photosphere coincide with the sonic point of the wind.

As the outer mass accretion rate increases, the winds become more massive, thereby reducing the fraction of mass accreted on to the black hole. Also, some of the dissipated energy is then advected with the flow into the BH.

For very high accretion rates surpassing about $20\dot{m}_{\rm crit}$, the photosphere which resides in the wind is found to be located at $z \gtrsim r$. This implies that the 1D+1D type of solution described here breaks down. Instead, one has to look for a solution in which the semihydrostatic inflow has a disc-like solution, while the supersonic outgoing wind has a spherical-like solution. The description

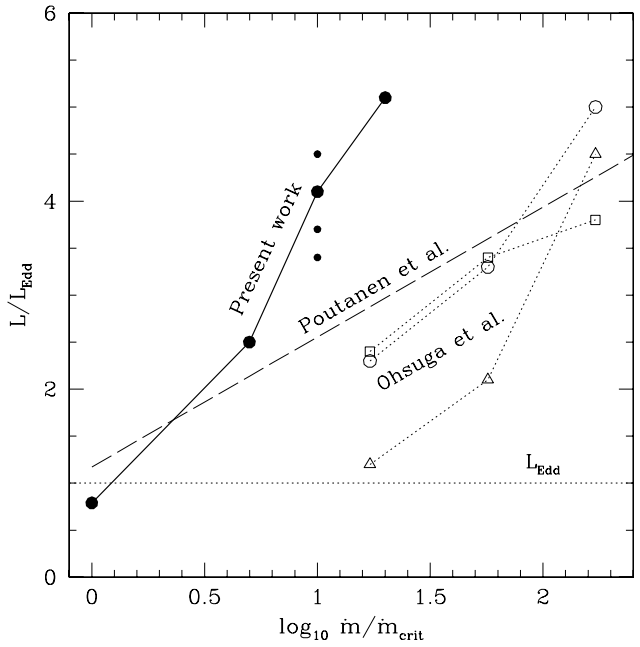

Figure 11. The total luminosity emitted as a function of the outer accretion rate. The black points denote the present results. The smaller points are the results of the sensitivity analysis. From top to bottom they correspond to the $p = 3, \alpha = 0.01$ and $\alpha = 0.1$ models. The dashed line corresponds to the L–$\dot{m}$ relation of Poutanen et al. (2007), while the open symbols, the results of Ohsuga et al. (2005) – squares with $Z = 0$, circles for $Z = Z_{\odot}$ and triangles for $Z = 10\,Z_{\odot}$. Note that the different values of $\dot{m}$ obtained by the different authors were scaled to the same $\dot{m}_{\rm crit}$ used here, which is $L_{\rm Edd}/0.057c^2$ (see equation 2).

of such extremely high accretion rate discs is the subject of a future publication.

One of the uncertainties in the model is the opacity law behaviour of the porous atmosphere. The reasons it is not known well is because it depends on the non-linear radiative hydrodynamic configuration the atmosphere will reach, and unfortunately, there are still no systematic studies of the saturation of the radiative-hydrodynamic or radiative-magneto-hydrodynamic instabilities, and how these reduce the effective opacity. Namely, there are no results yet from which one can write a $\kappa_{\rm eff}(\Gamma)$ law. For this reason we parametrized the effective opacity (see equation 22). A second uncertainty is the viscosity, parametrized using the α-model.

Fortunately, the disc characteristics were found to be mostly insensitive to the model uncertainties. The insensitivity to α can be understood in the standard way. Changing α while keeping $\dot{m}$ implies that the density at each radius adjusts itself such that the resulting angular momentum loss will be that required to accrete the given $\dot{m}$. The effects of changing the opacity law is likely to be similar. Relations for which the wind mass-loss rate at a given radius is smaller imply that more mass will reach smaller radii. This will release more energy, and therefore drive a larger mass-loss rate to compensate. We can conclude therefore that the model uncertainties do not undermine the model predictions. On the other hand, it would be impossible to use SED accretion discs to constrain the characteristics of porous atmospheres.

ACKNOWLEDGMENT

NJS is grateful to the support of ISF grant 1589/10.

REFERENCES

Abamowicz M. A., Piran T., 1980, ApJ, 241, L7
Abramowicz M. A., Czerny B., Lasota J. P., Szuszkiewicz E., 1988, ApJ, 332, 646
Abramowicz M. A., Chen X., Kato S., Lasota J., Regev O., 1995, ApJ, 438, L37
Arons J., 1992, ApJ, 388, 561
Bardeen J. M., 1973, in A. Giannaras, ed., Black Holes (Les Astres Occlus), p. 215
Begelman M. C., 2002, ApJ, 568, L97
Begelman M. C., 2006, ApJ, 643, 1065
Blandford R. D., Begelman M. C., 1999, MNRAS, 303, L1
Davis S. W., Blaes O. M., Hubeny I., Turner N. J., 2005, ApJ, 621, 372
Eggum G. E., Coroniti F. V., Katz J. I., 1988, ApJ, 330, 142
Gammie C. F., 1998, MNRAS, 297, 929
Glatzel W., 1994, MNRAS, 271, 66
Ichimaru S., 1977, ApJ, 214, 840
Jaroszynski M., Abramowicz M. A., Paczynski B., 1980, Acta Astron., 30, 1
Joss P. C., Salpeter E. E., Ostriker J. P., 1973, ApJ, 181, 429
Narayan R., Yi I., 1994, ApJ, 428, L13
Ohsuga K., Mori M., Nakamoto T., Mineshige S., 2005, ApJ, 628, 368
Owocki S. P., Gayley K. G., 1997, in Nota A., Lamers H., eds, ASP Conf. Ser. Vol. 120, Luminous Blue Variables: Massive Stars in Transition. Astron. Soc. Pac., San Francisco, p. 121
Owocki S. P., Gayley K. G., Shaviv N. J., 2004, ApJ, 616, 525
Paczynsky B., Wiita P. J., 1980, A&A, 88, 23
Papaloizou J. C. B., Alberts F., Pringle J. E., Savonije G. J., 1997, MNRAS, 284, 821
Poutanen J., Lipunova G., Fabrika S., Butkevich A. G., Abolmasov P., 2007, MNRAS, 377, 1187
Schwarz G. J., Shore S. N., Starrfield S., Hauschildt P. H., Della Valle M., Baron E., 2001, MNRAS, 320, 103
Shakura N. I., Sunyaev R. A., 1973, A&A, 24, 337
Shaviv N. J., 1998, ApJ, 494, L193
Shaviv N. J., 2000, ApJ, 532, L137
Shaviv N. J., 2001a, ApJ, 549, 1093
Shaviv N. J., 2001b, MNRAS, 326, 126
Shaviv G., Wickramasinghe D., Wehrse R., 1999, A&A, 344, 639
Starrfield S., 1989, in Bode M. F., Evans A., eds, Classical Novae. Wiley, Chichester
Titarchuk L., 1994, ApJ, 434, 570
Turner N. J., Blaes O. M., Socrates A., Begelman M. C., Davis S. W., 2005, ApJ, 624, 267
van Marle A. J., Owocki S. P., Shaviv N. J., 2009, MNRAS, 394, 595

This paper has been typeset from a TEX/LATEX file prepared by the author.